ELSEVIER

Computers in Biology and Medicine 38 (2008) 1–13

Computers in Biology and Medicine

www.intl.elsevierhealth.com/journals/cobm

ECG signal denoising and baseline wander correction based on the empirical mode decomposition

Manuel Blanco-Velasco[a,*], Binwei Weng[b], Kenneth E. Barner[c]

[a]*Department of Teoría de la Señal y Comunicaciones, Universidad de Alcalá, Campus Universitario, 28871 Alcalá de Henares, Madrid, Spain*
[b]*Philips Medical Systems, Andover, MA 01810, USA*
[c]*Department of Electrical and Computer Engineering, University of Delaware, Newark, DE 19716, USA*

Received 18 July 2006; received in revised form 10 May 2007; accepted 18 June 2007

Abstract

The electrocardiogram (ECG) is widely used for diagnosis of heart diseases. Good quality ECG are utilized by physicians for interpretation and identification of physiological and pathological phenomena. However, in real situations, ECG recordings are often corrupted by artifacts. Two dominant artifacts present in ECG recordings are: (1) high-frequency noise caused by electromyogram induced noise, power line interferences, or mechanical forces acting on the electrodes; (2) baseline wander (BW) that may be due to respiration or the motion of the patients or the instruments. These artifacts severely limit the utility of recorded ECGs and thus need to be removed for better clinical evaluation. Several methods have been developed for ECG enhancement. In this paper, we propose a new ECG enhancement method based on the recently developed empirical mode decomposition (EMD). The proposed EMD-based method is able to remove both high-frequency noise and BW with minimum signal distortion. The method is validated through experiments on the MIT–BIH databases. Both quantitative and qualitative results are given. The simulations show that the proposed EMD-based method provides very good results for denoising and BW removal.

Keywords: Electrocardiogram (ECG); Stress ECG; ECG enhancement; Empirical mode decomposition (EMD); Denoising; Baseline wander; Baseline drift

1. Introduction

The electrocardiogram (ECG) is the recording of the cardiac activity and it is extensively used for diagnosis of heart diseases. It is also an essential tool to allow monitoring patients at home, thereby advancing telemedical applications. Recent contributions in this topic are reported in [1–3]. Even though these contributions are for different projects, the issue common to each is the use of ECG for remote monitoring and assistance under different telecommunication platforms. The transmission of ECG often introduces noise due to poor channel conditions. Moreover, there are other types of noise inherent in the data collection process. These artifacts are particularly significant during a stress test. The main sources of such artifacts are: (1) the baseline wander (BW) mainly caused by respiration, and (2) high-frequency noise such as the electromyographic (EMG) noise caused by the muscle activity. Moreover, the motion of the patient or the leads affects both types of artifacts. In ECG enhancement, the goal is to separate the valid ECG from the undesired artifacts so as to present a signal that allows easy visual interpretation.

Many approaches have been reported in the literature to address ECG enhancement. Some recent relevant contributions have proposed solutions using a wide range of different techniques, such as perfect reconstruction maximally decimated filter banks [4] and nonlinear filter banks [5], advanced averaging [6,7], the wavelet transform [8–11], adaptive filtering [12], singular value decomposition [13], and independent component analysis [14].

In this paper, we propose a new method for ECG enhancement based on the empirical mode decomposition (EMD). The EMD was recently introduced in [15] as a technique for processing nonlinear and nonstationary signals. It also serves as an alternative to methods such as the wavelet analysis, the

* Corresponding author. Tel.: +34 91 885 67 08.
E-mail addresses: manuel.blanco@uah.es (M. Blanco-Velasco), binwei.weng@philips.com (B. Weng), barner@ece.udel.edu (K.E. Barner).

0010-4825/$ - see front matter © 2007 Elsevier Ltd. All rights reserved.
doi:10.1016/j.compbiomed.2007.06.003

Wigner–Ville distribution, and the short-time Fourier transform. It is proposed as a preprocessing stage to efficiently compute the instantaneous frequency through the Hilbert transform [16], although it can be applied independently as well.

It is reported in [17] that EMD behaves as a "wavelet-like" dyadic filter bank for fractional Gaussian noise. This conclusion has been applied in a detrending and denoising example in [18]. The work in [19] presents one of the first application of EMD in biomedical engineering, where blood pressure is studied. Regarding ECG signal processing, one of the first EMD-based contributions is [20], which investigates the chaotic nature of ECG. Also related to the cardiac system, the EMD is utilized in the analysis of heart rate variability (HRV) [21,22]. The EMD is also used for artifact reduction in gastric signals [23]. Finally, in [24], the EMD is utilized to extract the lower esophageal sphincter pressure in the gastroesophageal reflux disease.

As the brief review above demonstrates, the EMD is a good tool for artifact reduction applications. This motivates the proposed use of the EMD for ECG enhancement. In this work, we address both denoising and BW removal based on the EMD.

The contributions of this work lie in two aspects. First, we introduce the use of the EMD in ECG enhancement. Second, noting that both high-frequency noise and BW components are mixed with ECG signal component in the EMD domain, we develop novel methods to remove both types of artifacts.

The performance of the proposed algorithm is demonstrated through various experiments performed over several records from the MIT–BIH arrhythmia database [25]. Quantitative and qualitative experiments are carried out for synthetic and real noise cases. The experimental studies show that the proposed EMD-based method is a good tool for ECG denoising and BW removal, especially for the important real noise cases.

The outline of the paper is as follows. In Section 2 a brief review of the EMD is presented. The algorithms for denoising and baseline removal are explained in Sections 3 and 4, respectively. Section 5 presents the experimental studies that demonstrate the performances of the proposed method. Finally, conclusions are given in Section 6.

2. Empirical mode decomposition

The EMD was recently proposed by Huang et al. [15] as a tool to adaptively decompose a signal into a collection of AM–FM components. Traditional data analysis methods, like Fourier and wavelet-based methods, require some predefined basis functions to represent a signal. The EMD relies on a fully data-driven mechanism that does not require any *a priori* known basis. It is especially well suited for nonlinear and nonstationary signals, such as biomedical signals.

The aim of the EMD is to decompose the signal into a sum of intrinsic mode functions (IMFs). An IMF is defined as a function with equal number of extrema and zero crossings (or at most differed by one) with its envelopes, as defined by all the local maxima and minima, being symmetric with respect to zero. An IMF represents a simple oscillatory mode as a counterpart to the simple harmonic function used in Fourier analysis.

Given a signal $x(t)$, the starting point of the EMD is the identification of all the local maxima and minima. All the local maxima are then connected by a cubic spline curve as the upper envelope $e_u(t)$. Similarly, all the local minima are connected by a spline curve as the lower envelope $e_l(t)$. The mean of the two envelopes is denoted as $m_1(t) = [e_u(t) + e_l(t)]/2$ and is subtracted from the signal. Thus, the first proto-IMF $h_1(t)$ is obtained as

$$h_1(t) = x(t) - m_1(t). \tag{1}$$

The above procedure to extract the IMF is referred to as the sifting process. Since $h_1(t)$ still contains multiple extrema in between zero crossings, the sifting process is performed again on $h_1(t)$. This process is applied repetitively to the proto-IMF $h_k(t)$ until the first IMF $c_1(t)$, which satisfies the IMF condition, is obtained. Some stopping criteria are used to terminate the sifting process. A commonly used criterion is the sum of difference (SD) [16]:

$$\mathrm{SD} = \sum_{t=0}^{T} \frac{|h_{k-1}(t) - h_k(t)|^2}{h_{k-1}^2(t)}. \tag{2}$$

When the SD is smaller than a threshold, the first IMF $c_1(t)$ is obtained, which is written as

$$r_1(t) = x(t) - c_1(t). \tag{3}$$

Note that the residue $r_1(t)$ still contains some useful information. We can therefore treat the residue as a new signal and apply the above procedure to obtain

$$\begin{aligned} &r_1(t) - c_2(t) = r_2(t), \\ &\vdots \\ &r_{N-1}(t) - c_N(t) = r_N(t). \end{aligned} \tag{4}$$

The whole procedure terminates when the residue $r_N(t)$ is either a constant, a monotonic slope, or a function with only one extremum. Combining the equations in (3) and (4) yields the EMD of the original signal:

$$x(t) = \sum_{n=1}^{N} c_n(t) + r_N(t). \tag{5}$$

The result of the EMD produces N IMFs and a residue signal. For convenience, we refer to $c_n(t)$ as the nth-order IMF. By this convention, lower-order IMFs capture fast oscillation modes while higher-order IMFs typically represent slow oscillation modes. If we interpret the EMD as a time-scale analysis method, lower-order IMFs and higher-order IMFs correspond to the fine and coarse scales, respectively. The residue itself can also be regarded as an IMF, which brings some convenience in the development presented below.

3. ECG denoising using EMD

High-frequency denoising by the EMD is in general carried out by partial signal reconstruction, which is premised on the fact that noise components lie in the first several IMFs. This

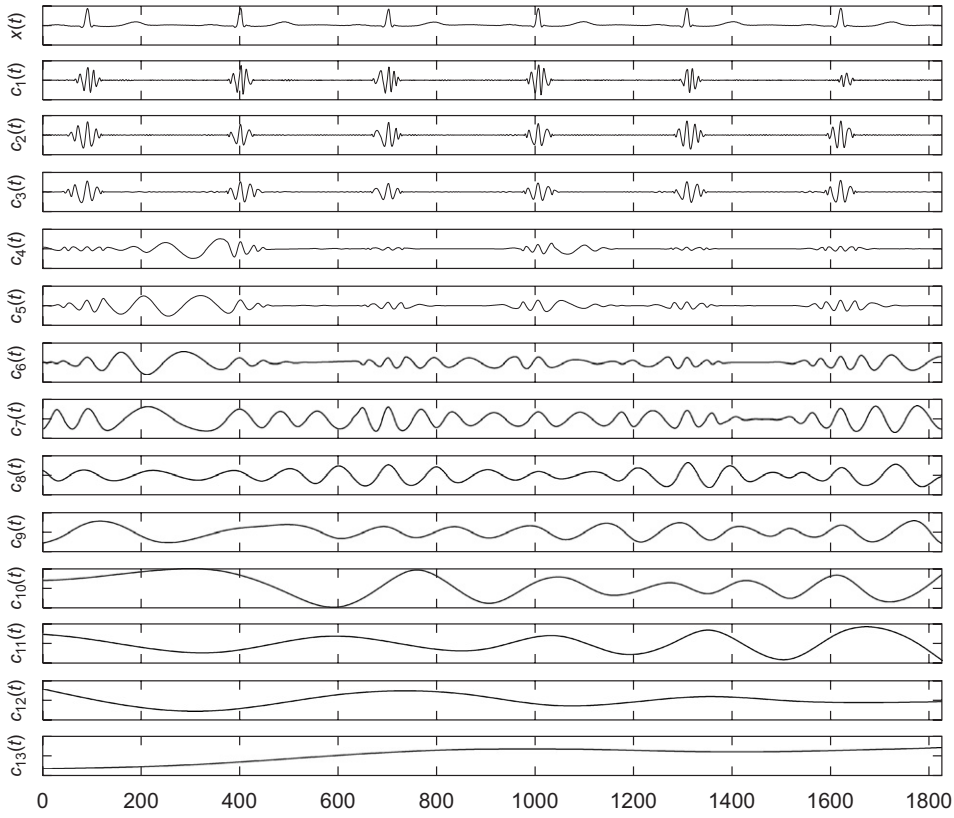

Fig. 1. EMD of a clean ECG. From top to bottom: clean ECG and resulting IMF 1–13. Vertical axes of subplots are not in the same scale.

strategy works well for those signals whose frequency content is clearly distinguished from that of noise and is successfully applied in [18,24]. The basic idea is to statistically determine the index of the IMFs that contain most of the noise components, beginning from fine to coarse scale. Given the index, the IMFs corresponding to the noise are removed and the reconstruction of the original signal is obtained by summing up the remaining IMFs. However, this approach cannot be assumed in the ECG case because the QRS complex spreads over the lower-order IMFs. Therefore, in the ECG case, EMD-based denoising requires a different strategy.

Noise encountered in ECG applications is usually located in the high-frequency band. Although most ECG signal power is concentrated in lower frequencies, the QRS complex spreads across the mid- to high-frequency bands. This complicates ECG denoising since lowpass filtering or simply removing lower-order IMFs will introduce severe QRS complex distortion, e.g., R-wave amplitude attenuation. As Section 2 illustrates, the EMD decomposes a signal into IMFs with decreasing frequency content. The EMD of clean and noisy ECG records are illustrated in the following two examples, thus revealing specific patterns associated with the QRS complex and noise in the EMD domain.

Consider first a clean ECG signal (first lead of record 103) from the MIT–BIH arrhythmia database decomposed by the EMD as shown in Fig. 1. The top plot shows the original ECG, and the remaining show all the IMFs from low to high orders. As we can see, the frequency content of each individual IMF decreases as the order of IMF increases. Note that the oscillatory patterns observed in the first three IMFs are mainly due to the QRS complex, which has strong high-frequency components. This observation can be used to delineate the QRS complex.

Consider next the EMD of a noisy ECG. A representative noisy signal is obtained by adding Gaussian noise to the clean signal in Fig. 1, the result of which is shown in the top graph of Fig. 2. The IMFs of the noisy signal are also shown in Fig. 2. Compared to the clean signal case, the first IMF of the noisy signal contains strong noise components. The oscillatory patterns of the QRS complex become more apparent starting from the second IMF. An analysis of EMD on clean and noisy ECG indicates that it is possible to filter the noise and at the same time preserve the QRS complex by temporal processing in the EMD domain. Multiple evaluations show these characteristics for all EMD decompositions of ECG signals. Therefore, the following four steps constitute the proposed denoising procedure:

(1) Delineate and separate the QRS complex.
(2) Use proper windowing to preserve the QRS complex.
(3) Use statistical tests to determine the number of IMFs contributing to the noise.
(4) Filter the noise by partial reconstruction.

These steps are detailed in the following.

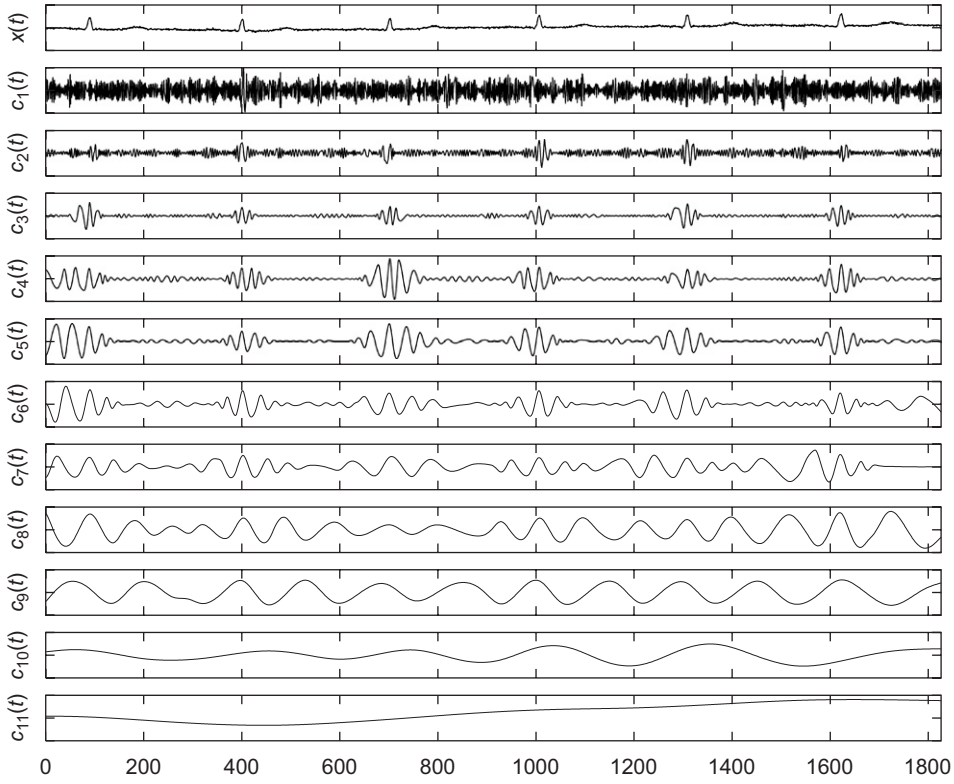

Fig. 2. EMD of a noisy ECG. From top to bottom: noisy ECG and its IMF 1–11. Vertical axes of subplots are not in the same scale.

3.1. Delineation of the QRS complex

To preserve the QRS complex, we need a delineation of the QRS complex. The oscillatory patterns in the first several IMFs indicate a link between these patterns and the QRS complex. Therefore, the first several IMFs can be jointly used to delineate the QRS complex. Our scheme utilizes the first three IMFs. That is, they are summed together to yield a signal which is used for delineation. Experiments show that this three term partial sum is sufficient to delineate the QRS complex.

The QRS complex and the oscillatory patterns in the first three IMFs are illustrated in the example of Fig. 3 for both clean and noisy ECG signals. In these two figures, the ECG signal is plotted in a solid line and the dash-dotted line is the sum of the first three IMFs: $d(t)=c_1(t)+c_2(t)+c_3(t)$. A close examination of Fig. 3(a) reveals that the QRS complex is bounded by the two zero-crossing points of $d(t)$. One zero-crossing point is on the left-hand side of the local minimum near the fiducial point (R-wave) and the other is on the right- hand side of the local minimum near the fiducial point, as shown in Fig. 3(a). Even in the noisy case (Fig. 3(b)), this relation holds, which shows that the usage of the three IMFs is a valid choice in the sense that it is less affected by the noise.

Given the sum of the first three IMFs $d(t)$, we can delineate the QRS complex through the following procedure:

(1) Identify the fiducial points.
(2) Apply the EMD to the noisy ECG signal. Sum the first three IMFs to obtain $d(t)$.
(3) Find the two nearest local minima on both sides of the fiducial.
(4) Detect the two closest zero-crossing points on the left-hand side of the left minimum and on the right-hand side of the right minimum. These two points are identified as boundaries of the QRS complex.

Here, and in the remainder of the paper, we assume that the fiducial points are either known (for example, by annotation) or can be determined by some other methods.

3.2. Windowing to preserve the QRS complex

Next, a window function is designed to preserve the QRS complex. The window function is a time domain window applied to the first several IMFs corresponding to the noise. A general design guideline for the QRS preserving window function is that it should be flat over the duration of the QRS complex and decay gradually to zero so that a smooth transition introduces minimal distortion. Since the window size is determined by the delineation results in the first step, these window functions adjust their sizes according to the QRS duration. A typical window function, and that which is used here, is the Tukey window (tapered cosine window):

$$w(t)=\begin{cases}\dfrac{1}{2}\left[1+\cos\left(\pi\dfrac{|t|-\tau_1}{\tau_2-\tau_1}\right)\right], & \tau_1\leqslant|t|\leqslant\tau_2,\\ 1, & |t|<\tau_1,\\ 0, & |t|>\tau_2,\end{cases} \tag{6}$$

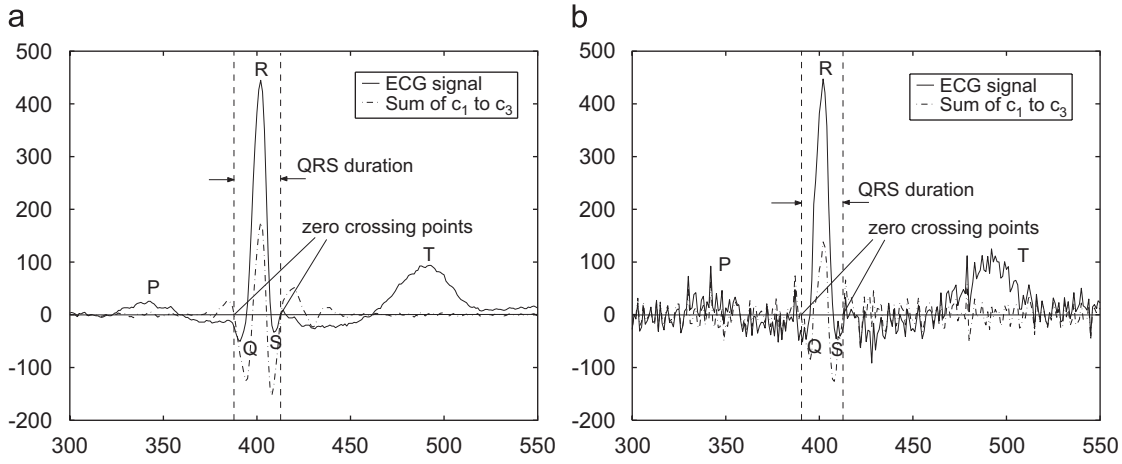

Fig. 3. Delineation of the QRS complex in the EMD domain. The solid line is the ECG signal and the dash-dotted line is the sum of the first three IMFs: $c_1(t)+c_2(t)+c_3(t)$. (a) Clean ECG, (b) noisy ECG.

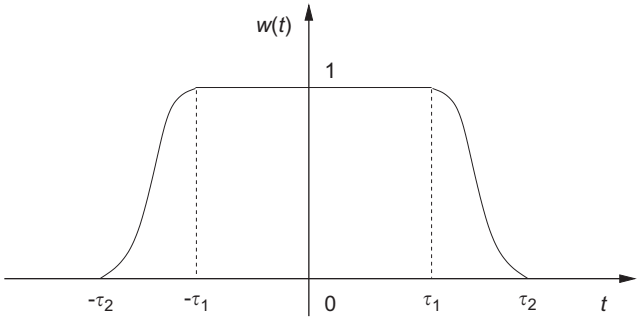

Fig. 4. Tukey window (tapered cosine) function.

where τ_1 is the flat region limit and τ_2 is the transition region limit. The graphical representation of the Tukey window is shown in Fig. 4.

When using (6), the flat region width $2\tau_1$ is chosen such that it equals the QRS complex boundary determined by the method in Section 3.1. The transition region is set to avoid abrupt "cutoff" of the window and reduce the distortions. As shown in Figs. 1 and 2, the spread of the oscillatory pattern around the QRS complex increases with the IMF order. Consequently, a variable width transition region in (6) is adopted to cope with the spreading effect of the various IMFs. We define the ratio between the one-sided transition region length $|\tau_1-\tau_2|$ and the flat region length $2\tau_1$ as

$$\beta = \frac{|\tau_1 - \tau_2|}{2\tau_1}, \tag{7}$$

where β is a free parameter. For example, for the first IMF, β can be set to be 30%. Likewise, for the jth IMF, β is chosen as $j \times 30\%$, which indicates that the window itself spreads as the QRS complex spreads with increasing order of IMF.

3.3. Determination of noise order by statistical test

The number of the IMFs that are dominated by noise, referred to as the *noise order*, must be established. For ECG signals, the contaminating noise is usually zero mean while the signal is nonzero mean. This fact enables the noise and signal to be separated in the EMD domain. Since lower-order IMFs contain the noise, we perform a statistical test to determine if a particular combination of IMFs has zero mean. An example of such a test is the t-test, which is also used in [24] to identify the noise-contributing IMFs.

The t-test is able to establish if the mean of the IMF deviates from zero. In the t-test, we perform the following hypothesis testing:

$$\begin{aligned} &\mathrm{H}_0: \quad \mathrm{mean}(c_{\mathrm{PS}}^M(t)) = 0, \\ &\mathrm{H}_1: \quad \mathrm{mean}(c_{\mathrm{PS}}^M(t)) \neq 0, \end{aligned} \tag{8}$$

where c_{PS}^M is the Mth-order partial sum of the IMFs:

$$c_{\mathrm{PS}}^M(t) = \sum_{i=1}^{M} c_i(t). \tag{9}$$

By selecting a certain significance level α, the null hypothesis H_0 is rejected in favor of the alternative hypothesis H_1 if the p value is less than α. Thus, starting from the first IMF, we perform a t-test on the partial sum $c_{\mathrm{PS}}^M(t)$ for $M = 1, 2, \ldots$ until we obtain a partial sum $c_{\mathrm{PS}}^{P_t}(t)$ that accepts the alternative hypothesis. The IMF order P_t at the termination point indicates that there are P_t IMFs that contribute primarily to the noise, and is thus set as the noise order. The role of the noise order in the EMD-based method is similar to the cutoff frequency in frequency domain filtering, and indicates how many IMFs should be removed.

In some cases the ECG itself has a mean close to zero. Using the previous technique to determine the noise order in such cases results in oversmoothing or loss of information since the

noise order will be very large. To avoid this potential problem, the noise order is set as

$$P = \min(P_t, 5), \tag{10}$$

where P_t is the noise order obtained from the t-test. The rationale for (10) is that IMFs with order higher than five typically contain little or no noise. Thus, this approach avoids the oversmoothing problem without sacrificing noise removal.

3.4. Denoising by partial reconstruction

Having established a method to determine the noise order, we can filter the noise by partial IMF reconstruction. To preserve the QRS complex, the window functions are applied to the P IMFs considered to be noise components. For the ith IMF, a window function $\psi_i(t)$ is constructed by concatenating the window functions (6), each of which centered at the QRS complex is applied. Mathematically,

$$\psi_i(t) = \sum_{j=1}^{N_r} w_{ij}(t), \tag{11}$$

where N_r is the number of QRS complex and $w_{ij}(t)$ denotes the variable size window for the jth QRS complex in the ith IMF. The aim of the window function $\psi_i(t)$ is to eliminate the noise and retain the QRS complex. To further reduce the distortion, we define the complementary window function which is given by

$$\bar{\psi}_i(t) = 1 - \psi_i(t), \quad \forall t. \tag{12}$$

Clearly, $\bar{\psi}_i(t)$ suppresses the QRS complex and retains some noise information. Its effect is contrary to that of $\psi_i(t)$. Here, $\bar{\psi}_i(t)$ is applied to the first P IMFs in conjunction with $\psi_i(t)$. The main reason of using the complementary window function is to avoid abrupt changes to the QRS complex by allowing a negligible amount of noise components in the lower-order IMFs. The sum of the P windowed IMFs, the remaining $N - P$ IMFs, and the residue forms the reconstructed signal:

$$\hat{x}(t) = \sum_{i=1}^{P} \psi_i(t)c_i(t) + \sum_{i=1}^{P} a_i\bar{\psi}_i(t)c_i(t) + \sum_{i=P+1}^{N} c_i(t) + r_N(t), \tag{13}$$

where $0 < a_i < 1$ is the attenuation coefficient. Typically a_i can be chosen between 0.1 and 0.3.

4. ECG BW removal using EMD

Since BW is a low-frequency phenomenon, it is expected that the major BW components are located in the higher-order IMFs. The residue, which can also be regarded as the last IMF, may not correspond to the BW because the BW may have multiple extrema and zero crossings, which violates the residue definition. Indeed, the BW spreads over the last several IMFs. Simply removing the last several IMFs may introduce significant distortions. Thus, the BW must be separated from the desired components in the last several IMFs. Moreover, as in the denoising case, the number of IMFs that contribute to the BW must be established. This number is referred to as BW *order*.

To remove the BW, a BW estimate is first obtained via a "multiband" filtering approach. The estimated BW is then subtracted from the signal, yielding the reconstructed signal. A bank of lowpass filters are applied to the last several IMFs. The sum of the output of this filterbank serves as the BW estimate.

Suppose the signal with BW is $x(t)$. After performing the EMD, we obtain all the IMFs:

$$x(t) = \sum_{i=1}^{N+1} c_i(t), \tag{14}$$

where the residue is included in the summation as the last IMF, $c_{N+1}(t)$. Denote the BW order as Q. We design a bank of lowpass filters $h_i(t)$, $i = 1, 2, \ldots, Q$, and then filter the IMFs starting from the last, $c_{N+1}(t)$, by these lowpass filters. The outputs of these filters are

$$\begin{aligned} b_1(t) &= h_1(t) * c_{N+1}(t), \\ b_2(t) &= h_2(t) * c_N(t), \\ &\vdots \\ b_Q(t) &= h_Q(t) * c_{N-Q+2}(t), \end{aligned} \tag{15}$$

where $*$ denotes the convolution. The cutoff frequencies of the lowpass filters are chosen as follows. Set the cutoff frequency of the first lowpass filter $h_1(t)$ to be ω_0. The cutoff frequency of the kth filter is set as

$$\omega_k = \frac{\omega_0}{M^{k-1}}, \tag{16}$$

where $M > 1$ is a frequency-folding number. The cutoff frequencies are related in this fashion due to the fact that, as the IMF order decreases, fewer BW components, but more signal components, are present in the IMF. This multiband filtering scheme considers each IMF as a subband of the signal and performs filtering on each subband.

The output $b_i(t)$ extracts the BW component in each IMF. Therefore, it can be used to determine the BW order Q. The variance of each $b_i(t)$ is determined as

$$\mathrm{var}\{b_i(t)\} = \frac{1}{L-1}\sum_{t=0}^{L-1}[b_i(t) - \mu_{b_i}]^2, \tag{17}$$

where μ_{b_i} is the mean value of $b_i(t)$. Starting from the last IMF, we choose Q such that $\mathrm{var}\{b_{Q+1}(t)\} < \zeta$ and $\mathrm{var}\{b_Q(t)\} \geqslant \zeta$, where ζ is an appropriate established threshold. The selection of the parameters ω_0, M, ζ can be based on *a priori* knowledge or can be experimentally tuned according to the BW behavior. In the later simulations, some typical values are given for these parameters.

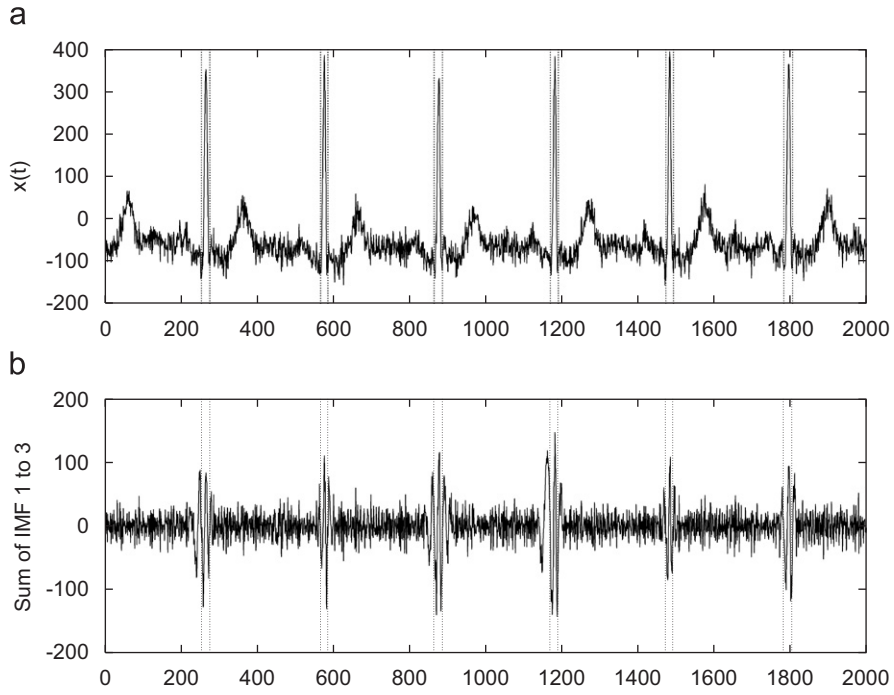

Fig. 5. QRS complex delineation results. The delineated boundaries are shown in dashed lines. (a) Noisy signal, (b) correspondence in the sum of the first three IMFs.

Once the BW order Q is determined, the outputs of all the filters are synthesized to form the estimate

$$\hat{b}(t) = \sum_{i=1}^{Q} b_i(t). \tag{18}$$

Finally, removing the BW yields the reconstructed signal

$$\tilde{x}(t) = x(t) - \hat{b}(t). \tag{19}$$

In the most general case, ECG signals are contaminated by both high-frequency noise and BW. The method of denoising in Section 3 and the method of removing BW in Section 4 can be combined to remove both artifacts. Because the noise only affects the lower-order IMFs while the BW only affects the higher-order IMFs, the methods do not interfere with each other. Consequently, the reconstructed signal after removing both high-frequency noise and BW is

$$\hat{x}(t) = \sum_{i=1}^{P} \psi_i(t) c_i(t) + \sum_{i=1}^{P} a_i \bar{\psi}_i(t) c_i(t) + \sum_{i=P+1}^{N+1} c_i(t) - \sum_{j=1}^{Q} h_j(t) * c_{N-j+2}(t), \tag{20}$$

where the residue $r_N(t)$ in (13) is rewritten as $c_{N+1}(t)$.

5. Experimental studies

In this section, simulations for several different cases are carried out to evaluate the performance of the proposed EMD-based method. A noisy signal $s(t) = x(t) + n(t)$ is processed to obtain an enhanced reconstructed version $\hat{x}(t)$. The corrupted signal $s(t)$ consists of an original clean signal $x(t)$, which is free of noise, and a noise component realization $n(t)$, that can be synthetic or real. Two groups of experiments are presented. The first simulation experiment is performed over synthetic noise and BW, where both qualitative and quantitative evaluations are given. In the second experiment, we study the real noise case.

In the following examples, all the ECG signals are from the MIT–BIH arrhythmia database. Every file in the database consists of two lead recordings sampled at 360 Hz with 11 bits per sample of resolution. The quantitative evaluation is assessed by the signal-to-error ratio (SER):

$$\mathrm{SER} = \frac{\sum_{t=0}^{L-1} x^2(t)}{\sum_{t=0}^{L-1} [x(t) - \hat{x}(t)]^2}, \tag{21}$$

where $x(t)$ is the original clean signal and $\hat{x}(t)$ is the reconstructed signal. The amount of noise in $s(t)$ is assessed by the signal-to-noise ratio (SNR):

$$\mathrm{SNR} = \frac{\sum_{t=0}^{L-1} x^2(t)}{\sum_{t=0}^{L-1} n^2(t)}, \tag{22}$$

where $n(t)$ is the noise realization.

5.1. Synthetic noise and BW

In this section, synthetic noise and BW are added to the signal from the first lead of record 103 from the MIT–BIH arrhythmia database. This signal is chosen because it captures normal sinus

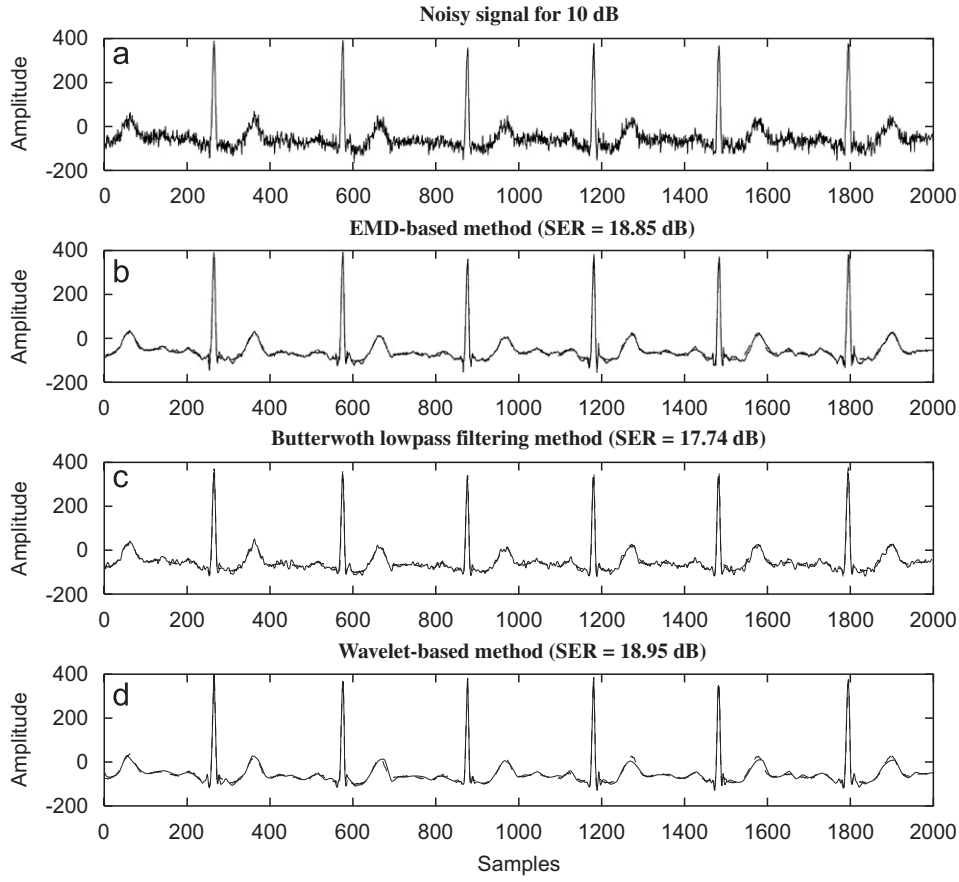

Fig. 6. ECG denoising for Gaussian noise. From top to bottom: (a) noisy signal for 10 dB, (b) EMD-based method (SER = 18.85 dB), (c) Butterworth lowpass filtering method (SER = 17.74 dB), (d) wavelet-based method (SER = 18.95 dB). The reconstructed signal (solid) and the original signal (dashed) are superimposed in the last three graphs for comparison purposes.

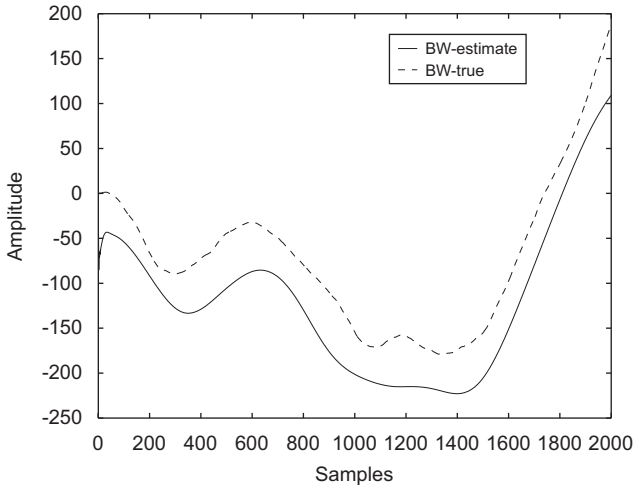

Fig. 7. BW estimation. Estimated BW (solid) vs. true baseline wander (dashed).

rhythms and is reasonably free of noise. The experiments cover three cases: Gaussian noise only, BW only, and both Gaussian noise and BW.

5.1.1. Gaussian noise

Gaussian noise is added to the original clean signal to yield a 10 dB SNR. The IMFs of the noisy signal are obtained by applying the EMD. Based on the relationship of the QRS complex and the oscillatory patterns revealed in Section 3.1, the QRS complex is delineated (Fig. 5). In the statistical t-test, the significance level α is set to be 0.01. Thus, the noise order P is determined to be four since at this level $p = 0.0019 < \alpha$. The transition parameter β in the window function is set to 30%. The attenuation coefficients a_i's for IMF 1–4 are set to be 0.1, 0.15, 0.2, 0.25. Finally, the reconstructed signal is obtained by (13). Fig. 6 shows the result. The top panel is the noisy signal and the following three panels show the reconstructed signals by the EMD; Butterworth lowpass filter, and wavelet-based methods. In the lowpass filtering method, the cutoff frequency is set to be 30 Hz, which is experimentally chosen to attain best denoising quality. In the wavelet-based method, the algorithm proposed in [8] is implemented for comparison. A 4-level discrete wavelet transform with the Cohen–Daubechies–Feauveau 9/7 (bior9.7) basis is used. The hard thresholding algorithm is applied to the DWT coefficients and the fixed threshold approach is chosen: the FIXTHRES method according to the notation in [8]. The SER for the reconstructed signals are 18.85 dB for

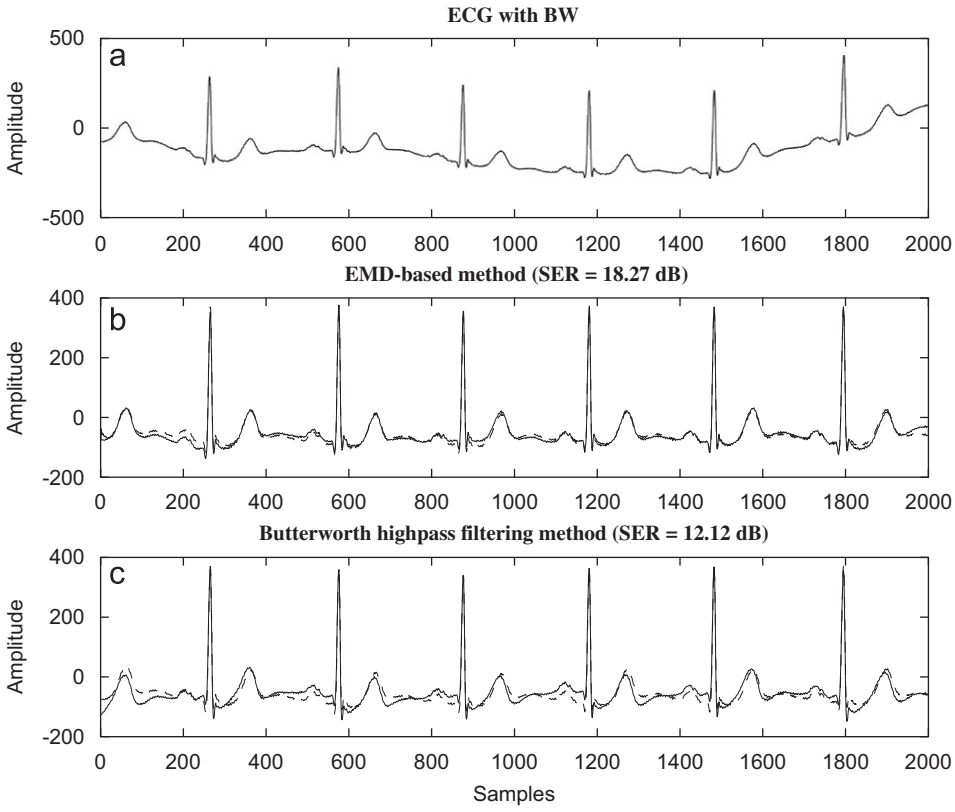

Fig. 8. ECG baseline wander removal. From top to bottom: (a) ECG with BW, (b) EMD-based method (SER = 18.27 dB), (c) Butterworth highpass filtering method (SER = 12.12 dB). In the last two graphs, the reconstructed signal (solid) and the original signal (dashed) are superimposed for comparison purposes.

the EMD-based method, 17.74 dB for the Butterworth filtering method, and 18.95 dB for the wavelet-based method. It can be seen that the proposed method achieves performance as similar to the wavelet-based method. This is only for the case of synthetic noise. For the later real noise case, the proposed method outperforms the wavelet-based method.

5.1.2. Baseline wander

We now focus on the case when only BW appears in the signal. To generate the synthetic BW, a Gaussian signal with variance on the order of the power of the original ECG signal is first generated. Then the resulting signal is passed through a lowpass filter. Adding the BW to the original ECG results in a signal with BW. The method proposed in Section 4 is utilized to estimate the BW. In the experiment, the parameters ω_0, M, and ζ are experimentally set to be 0.8, 20, and 10, respectively. The true and estimated BW are shown in Fig. 7. Note that the bias between the true and estimated BW is due to the DC offset removed by the EMD method and it is generally acceptable in ECG enhancement. We compare the proposed method with the Butterworth highpass filtering method. The cutoff frequency of highpass filter is experimentally set to be 0.09 Hz, which achieves best BW removal quality. The reconstructed signals by the proposed EMD-based method and the highpass filtering method are shown in Fig. 8. In terms of visual appearance, the EMD result contains less noticeable residual BW than the Butterworth highpass filtering result. Quantitatively, the EMD-based method yields an SER of 18.27 dB, which is significantly higher than 12.12 dB achieved by the highpass filtering method.

5.1.3. Both Gaussian noise and BW

As noted in Section 4, the proposed EMD-based method can be used for both denoising and BW removal. In this experiment, both Gaussian noise and BW are added to the original ECG. We follow the procedures in Sections 3 and 4 to remove the noise and BW. In the experiment, the same parameter as in Sections 5.1.1 and 5.1.2 are used. As a comparison, the Butterworth bandpass filtering method is implemented to remove both types of artifacts. The two cutoff frequencies of the bandpass filter are the cutoff frequencies of the lowpass and highpass filters used in the previous two experiments. The noisy and the reconstructed signals are shown in Fig. 9, from which we see that the performance of the EMD-based method is virtually identical to the cases in which the methods are applied to each case independently.

5.1.4. Quantitative evaluation

The previous examples show that the proposed methods yield very good results in terms of visual quality. In this example, we study the behavior of the method quantitatively, taking different signals from the database and using multiple realizations of Gaussian noise at different SNRs.

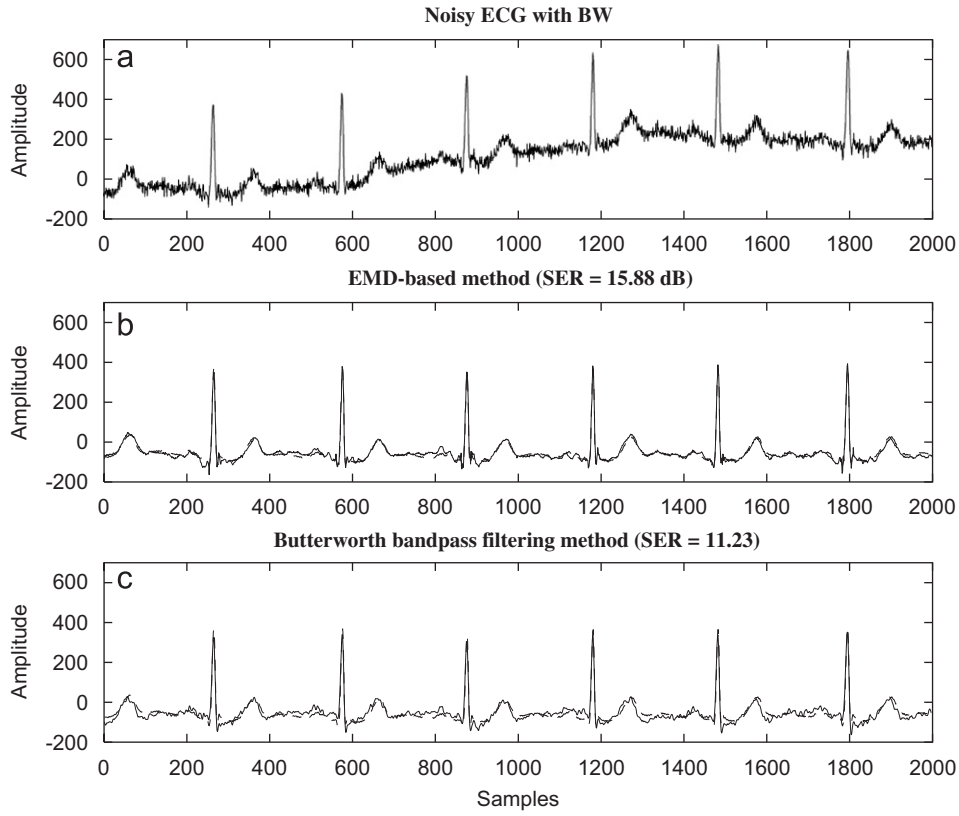

Fig. 9. ECG enhancement for Gaussian noise and BW. From top to bottom: (a) noisy ECG with BW, (b) EMD-based method (SER = 15.88 dB), (c) Butterworth bandpass filtering method (SER = 11.23 dB). In the last two graphs, the reconstructed signal (solid) and the original signal (dashed) are superimposed for comparison purposes.

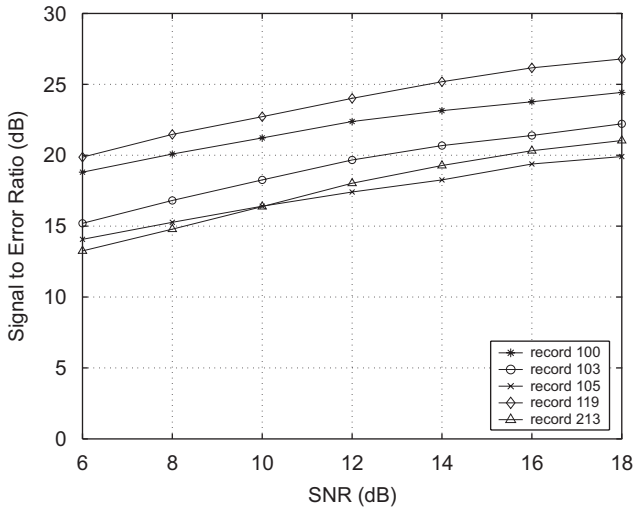

Fig. 10. SER (dB) vs. SNR (dB) for five signal records: 100, 103, 105, 119, and 213 in Gaussian noise case.

Five records are arbitrarily chosen from the MIT–BIH database, 100, 103, 105, 119, and 213. Also, the SNR of each record is ranged from 6 to 18 dB. At each SNR, 100 Monte Carlo runs are performed to obtain an averaged SER value. Results for the Gaussian noise cases are shown in Fig. 10. The horizontal axis in the plot corresponds to the input ECG SNR and the vertical axis shows the average SER of the reconstructed signals for the 100 runs. It can be seen that the SER improves as the SNR is increased.

5.2. Real noise experiment

In this experiment, we consider the ECG case corrupted by real noise. Here, the denoising is considered since the wavelet-based method is targeted for denoising. Two real noise records are taken from the MIT–BIH noise stress test database [25], the muscle artifact "ma" record and the electrode motion "em" record. The BW in each record is eliminated by lowpass filtering in order to provide quantitative results with (21).

Let $n_{\mathrm{ma}}(t)$ and $n_{\mathrm{em}}(t)$ be the "ma" and "em" BW free noise records, respectively. The total noise utilized to corrupt the original clean signal $x(t)$ is obtained as $n(t) = k_1 n_{\mathrm{ma}}(t) + k_2 n_{\mathrm{em}}(t)$, so that $k_i,\ i = 1, 2$, is chosen to contribute with the same SNR_0:

$$\mathrm{SNR}_0 = \frac{\sum_{t=0}^{L-1} x^2(t)}{\sum_{t=0}^{L-1} [k_1\ n_{\mathrm{ma}}(t)]^2} = \frac{\sum_{t=0}^{L-1} x^2(t)}{\sum_{t=0}^{L-1} [k_2\ n_{\mathrm{em}}(t)]^2}. \tag{23}$$

The resulting SNR is assessed with (22).

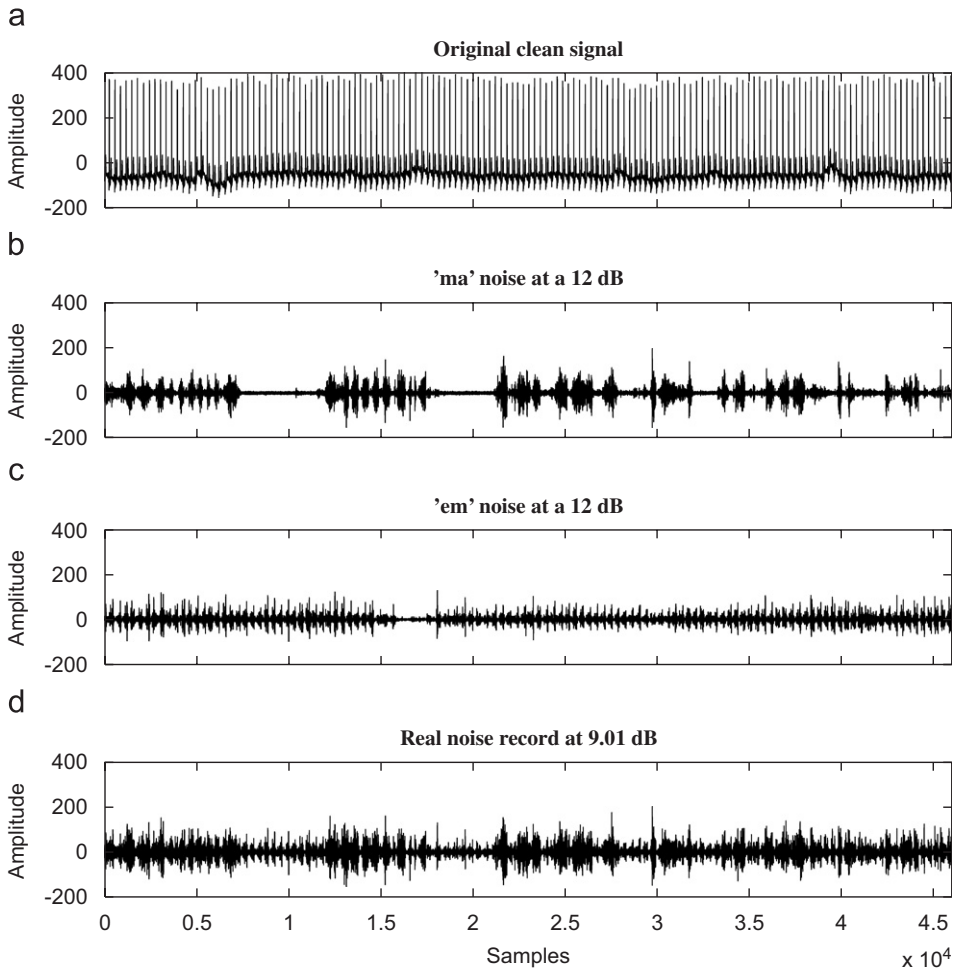

Fig. 11. Example of real noise added to clean signal. (a) Original signal (record 103), (b) "ma" noise, $SNR_0 = 12$ dB, (c) "em" noise, $SNR_0 = 12$ dB, (d) total noise $n(t)$ used to corrupt the original signal, SNR = 9.01 dB.

A long-term experiment is carried out to show how the proposed method works when a signal is processed under real conditions. The first 46,000 samples (corresponding to a bit more than 2 min) from an MIT noise free signal are used. The noisy signals are split into consecutive blocks to continuously process the long-term records (except in the lowpass filtering method).

Fig. 11 shows an example of the set of signals involved in this experiment. In Fig. 11(a), the 46,000-samples long noise free record from the MIT database is depicted (record 103). The noisy signal is obtained by adding the noise record in Fig. 11(d) attaining an SNR of 9.01 dB. The noise signal is obtained as the contribution of "ma" and "em" noise in Fig. 11(b) and (c), respectively, at an SNR_0 of 12 dB in both cases. In Fig. 12, the original, noisy, and reconstructed signals from the EMD-based, the Butterworth lowpass filtering, and the wavelet-based methods are displayed in the range of samples from 10,000 to 15,000, which has been arbitrarily chosen. The figure shows that the significant noise components are eliminated by the proposed method. However, both lowpass filtering and wavelet-based methods fail to remove the real noise satisfactorily. In addition, the SERs for the EMD-based, the Butterworth filtering, and the wavelet-based methods are calculated to be 12.27, 4.65, and 9.15 dB, respectively, which again confirms the superior performance of the proposed method when applied to the real noise. In the EMD-based method, the signal is processed in consecutive blocks of 2000 samples, and, as it can be seen in Fig. 12(c), the method does not introduce any distortion at the borders of consecutive segments.

Finally, the long-term test is repeated under the same circumstances with the records 100, 103, 105, 119, and 213 at different SNRs. The results are presented in Table 1 in terms of SER for the corresponding methods. As can be observed here once again, the wavelet-based method shows less ability to deal with real noise than the EMD-based method. We can see the behavior of the wavelet-based method in Fig. 12(e) where only few noise components are smoothed (see also Fig. 12(b) to compare), but it is unable to remove the strong noise components. These results further demonstrate that the proposed method is not only applicable to synthetic noise cases, but also suitable for real noise cases.

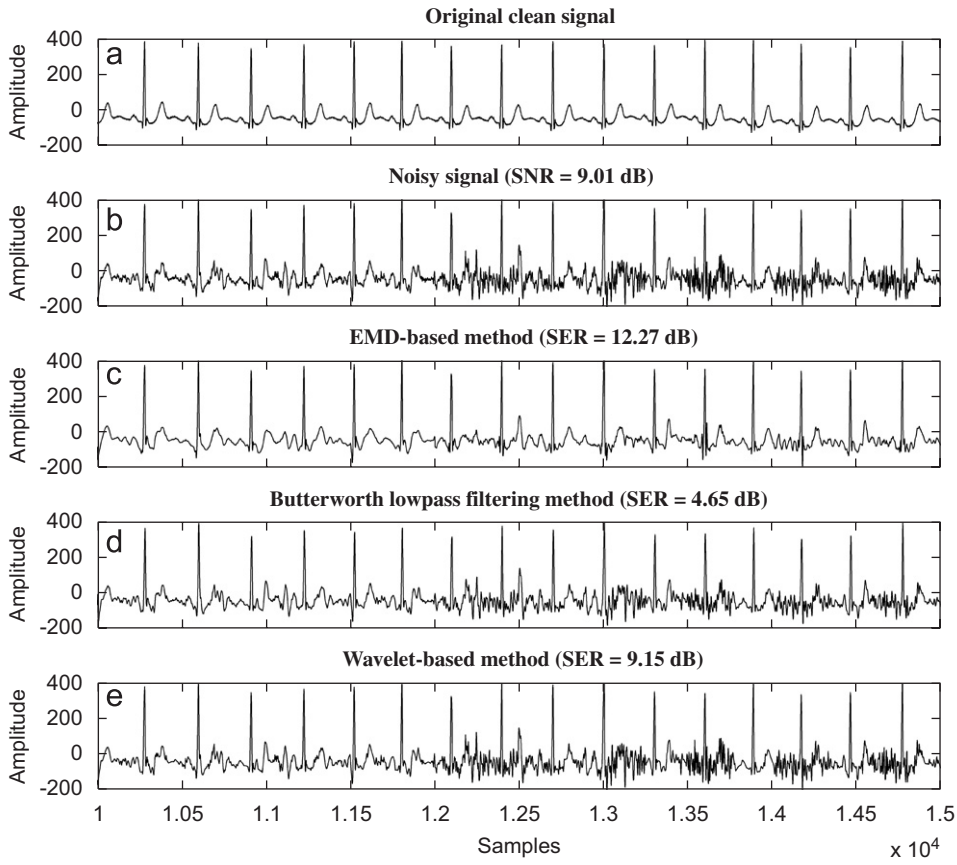

Fig. 12. ECG denoising for real noise. From top to bottom: (a) original signal (record 103), (b) noisy signal containing real noise, SNR = 9.01 dB, (c) EMD-based method, SER = 12.27 dB, (d) Butterworth lowpass filtering method, SER = 4.65 dB, (e) wavelet-based method, SER = 9.15 dB.

Table 1
Real noise long-term experiment carried out over several records from the MIT–BIH arrhythmia database

	SNR = 6 dB			SNR = 10 dB			SNR = 14 dB		
	SER_{emd} [a]	SER_{butt} [b]	SER_{wt} [c]	SER_{emd}	SER_{butt}	SER_{wt}	SER_{emd}	SER_{butt}	SER_{wt}
100	11.40	5.22	6.14	13.95	7.33	10.15	16.75	8.58	14.17
103	9.85	3.58	6.15	12.90	4.92	10.16	15.70	5.59	14.18
105	9.62	5.53	6.14	11.94	7.89	10.14	14.54	9.37	14.13
119	11.45	6.48	6.14	14.71	9.63	10.14	17.29	12.03	14.15
213	8.87	4.45	6.13	11.89	10.14	10.13	14.74	7.06	14.13

[a] SER value for the EMD-based method.
[b] SER value for the Butterworth lowpass filtering method.
[c] SER value for the wavelet-based method.

6. Conclusions

A novel method for ECG enhancement based on the EMD is presented. Both high-frequency noise and BW removal are addressed. Enhancement is achieved through the development of two EMD-based methods to address each type of artifact. The techniques developed are not based on simple partial summation of IMFs, as in previous work. Rather, different IMFs are chosen and processed to successfully achieve the denoising and BW removal. The effectiveness of the EMD in ECG enhancement is shown through several experiments that consider real and synthetic noise and BW. Results indicate that the EMD is an effective enhancement tool, especially for real noise and BW. The techniques used here can be applied in practical stress ECG tests and long-term Holter monitoring as in these cases strong noise and BW components are present in the recorded ECG.

Acknowledgment

M. Blanco-Velasco's work was supported in part by the Fondo de Investigación Sanitaria under project PI052277.

References

[1] K. Hung, Y.-T. Zhang, Implementation of a WAP-based telemedicine system for patient monitoring, IEEE Trans. Inf. Technol. Biomed. 7 (2) (2003) 101–107.

[2] C.H. Salvador, M.P. Carrasco, M.A.G. de Mingo, A.M. Carrero, J.M. Montes, L.S. Martín, M.A. Cavero, I.F. Lozano, J.L. Monteagudo, Airmed-cardio: a GSM and internet services-based system for out-of-hospital follow-up of cardiac patients, IEEE Trans. Inf. Technol. Biomed. 9 (1) (2005) 73–84.

[3] J. Rodríguez, A. Goñi, A. Illarramendi, Real-time classification of ECGs on a PDA, IEEE Trans. Inf. Technol. Biomed. 9 (1) (2005) 23–34.

[4] V.X. Afonso, W.J. Tompkins, T.Q. Nguyen, K. Michler, S. Luo, Comparing stress ECG enhancement algorithms, IEEE Eng. Med. Biol. Mag. 15 (3) (1996) 37–44.

[5] J.M. Leski, N. Henzel, ECG baseline wander and powerline interference reduction using nonlinear filter bank, Signal Process. 35 (4) (2004) 781–793.

[6] S. Iravanian, L. Tung, A novel algorithm for cardiac biosignal filtering based on filtered residue method, IEEE Trans. Biomed. Eng. 49 (11) (2002) 1310–1317.

[7] J.M. Leski, Robust weighted averaging, IEEE Trans. Biomed. Eng. 49 (8) (2002) 796–804.

[8] P.E. Tikkanen, Nonlinear wavelet and wavelet packet denoising of electrocardiogram signal, Biol. Cybern. 80 (4) (1999) 259–267.

[9] C.Y.-F. Ho, B.W.-K. Ling, T.P.-L. Wong, A.Y.-P. Chan, P.K.-S. Tam, Fuzzy multiwavelet denoising on ECG signal, Electron. Lett. 39 (16) (2003) 1163–1164.

[10] E. Ercelebi, Electrocardiogram signals de-noising using lifting-based discrete wavelet transform, Comput. Biol. Med. 34 (6) (2004) 479–493.

[11] S. Poornachandra, N. Kumaravel, Hyper-trim shrinkage for denoising of ECG signal, Digital Signal Process. 15 (3) (2005) 317–327.

[12] V. Almenar, A. Albiol, A new adaptive scheme for ECG enhancement, Signal Process. 75 (3) (1999) 253–263.

[13] J.S. Paul, M.R.S. Reddy, J. Kumar, Data processing of stress ECG using discrete cosine transform, Comput. Biol. Med. 28 (6) (1998) 639–658.

[14] A.K. Barros, A. Mansour, N. Ohnishi, Removing artifacts from electrocardiographic signals using independent components analysis, Neurocomputing 22 (1998) 173–186.

[15] N.E. Huang, Z. Shen, S.R. Long, M.C. Wu, H.H. Shih, Q. Zheng, N.-C. Yen, C.C. Tung, H.H. Liu, The empirical mode decomposition and Hilbert spectrum for nonlinear and nonstationary time series analysis, Proc. R. Soc. London 454 (1998) 903–995.

[16] N. Huang, N.O. Attoh-Okine, in: N. Huang, N.O. Attoh-Okine (Eds.), The Hilbert–Huang Transform in Engineering, CRC Press, Boca Raton, FL, 2005.

[17] P. Flandrin, G. Rilling, P. Goncalves, Empirical mode decomposition as a filter bank, IEEE Signal Process. Lett. 11 (2) (2004) 112–114.

[18] P. Flandrin, P. Goncalves, G. Rilling, Detrending and denoising with empirical mode decomposition, in: Proceedings of XII EUSIPCO 2004, Vienna, Austria, September 2004.

[19] W. Huang, Z. Shen, N.E. Huang, Y.C. Fung, Engineering analysis of biological variables: an example of blood pressure over 1 day, Proc. Nat. Acad. Sci. USA 95 (9) (1998) 4816–4821.

[20] J.I. Salisbury, Y. Sun, Assessment of chaotic parameters in nonstationary electrocardiograms by use of empirical mode decomposition, Ann. Biomed. Eng. 32 (10) (2004) 1348–1354.

[21] J.C. Echevarría, J.A. Crowe, M.S. Woolfson, B.R. Hayes-Gill, Application of empirical mode decomposition to heart rate variability analysis, Med. Biol. Eng. Comput. 39 (4) (2001) 471–479.

[22] R. Balocchi, D. Menicucci, E. Santarcangelo, L. Sebastiani, A. Gemignani, B. Ghelarducci, M. Varanini, Deriving the respiratory sinus arrhythmia from the heartbeat time series using empirical mode decomposition, Chaos Solitons Fractals 20 (1) (2004) 171–177.

[23] H. Liang, Z. Lin, R. McCallum, Artifact reduction in electrogastrogram based on empirical mode decomposition method, Med. Biol. Eng. Comput. 38 (1) (2000) 35–41.

[24] H. Liang, Q.-H. Lin, J.D.Z. Chen, Application of the empirical mode decomposition to the analysis of esophageal manometric data in gastroesophageal reflux disease, IEEE Trans. Biomed. Eng. 52 (10) (2005) 1692–1701.

[25] A.L. Goldberger, L.A.N. Amaral, L. Glass, J.M. Hausdorff, P.C. Ivanov, R.G. Mark, J.E. Mietus, G.B. Moody, C.-K. Peng, H.E. Stanley, PhysioBank, PhysioToolkit, and PhysioNet: components of a new research resource for complex physiologic signals, Circulation 101 (23) (2000) 215–220.

Manuel Blanco − Velasco was born in Saint Maur des Fossés, France, in 1967. He received the engineering degree from the Universidad de Alcalá, Madrid, Spain, in 1990, the MSc in communications engineering from the Universidad Politécnica de Madrid, Spain, in 1999, and the PhD degree from the Universidad de Alcalá in 2004. From 1992 to 2002, he was with the Circuits and Systems Department at the Universidad Politécnica de Madrid as Assistant Professor. In April 2002, he joined the Signal Theory and Communications Department of the Universidad de Alcalá where he is now working as Associate Professor. His main research interest is biomedical signal processing.

Binwei Weng received the BE and ME degrees in electrical engineering from Shanghai Jiao Tong University, Shanghai, China, in 1997 and 2000, respectively, and the MS degree in electrical and computer engineering from the University of Iowa, Iowa City, in 2003. He received his Ph.D. degree in Electrical and Computer Engineering from the University of Delaware in 2006. He is currently with Philips Medical Systems in Andover, Massachusetts. His main interests are nonlinear signal processing and biomedical signal processing.

Kenneth E. Barner received his B.S.E.E. degree (*magna cum laude*) from the Lehigh University, Bethlehem, Pennsylvania, in 1987. He received his M.S.E.E. and Ph.D. degrees from University of Delware, Newark, Delaware, in 1989 and 1992, respectively. For his dissertation "Permutation Filters: A Group Theoretic Class of Non-Linear Filters," Dr. Barner received the *Allan P. Colburn Prize in Mathematical Sciences and Engineering* for the most outstanding doctoral dissertation in the engineering and mathematical disciplines.

Dr. Barner was the duPont Teaching Fellow and a Visiting Lecturer at the University of Delaware in 1991 and 1992, respectively. From 1993 to 1997 Dr. Barner was an Assistant Research Professor in the Department of Electrical and Computer Engineering at the University of Delaware and a Research Engineer at the duPont Hospital for Children. He is currently a Professor in the Department of Electrical and Computer Engineering at the University of Delaware. Dr. Barner is the recipient of a 1999 NSF CAREER award. He was the co-chair of the *2001 IEEE-EURASIP Nonlinear Signal and Image Processing (NSIP) Workshop* and a Guest Editor for a special issue of the *EURASIP Journal of Applied Signal Processing on Nonlinear Signal and Image Processing*. Dr. Barner is a member of the Nonlinear Signal and Image Processing Board and is co-editor of the book *Nonlinear Signal and Image Processing: Theory, Methods, and Applications*, CRC Press, 2004. Dr. Barner was the Technical Program co-Chair for *ICASSP 2005* and is currently serving on the *IEEE Signal Processing Theory and Methods (SPTM)* and *IEEE Bio-Imaging and Signal Processing (BISP)* technical committees as well as the *IEEE Delaware Bay Section Executive Committee*. Dr. Barner has served as an Associate Editor of the *IEEE Transactions on Signal Processing, the IEEE Transaction on Neural Systems and Rehabilitation Engineering, and the IEEE Signal Processing Magazine*. Dr. Barner is currently the Editor-in-Chief of the journal *Advances in Human–Computer Interaction*, a member of the Editorial Board of the *EURASIP Journal of Applied Signal Processing*, and is serving as a Guest Editor for that journal on the *Super-Resolution Enhancement of Digital Video and Empirical Mode Decomposition and the Hilbert–Huang Transform* special issues. His research interests include signal and image processing, robust signal processing, nonlinear systems, communications, human–computer interaction, haptic and tactile methods, and universal access. Dr. Barner is a Member of Tau Beta Pi, Eta Kappa Nu, and Phi Sigma Kappa.